

# Propagation and Neural Regulation of Calcium Waves in Longitudinal and Circular Muscle Layers of Guinea Pig Small Intestine

RANDEL J. STEVENS, NELSON G. PUBLICOVER, and TERENCE K. SMITH

Biomedical Engineering Program, Department of Physiology and Cell Biology, University of Nevada School of Medicine, Reno, Nevada

**Background & Aims:** The relative movements of longitudinal muscle (LM) and circular muscle (CM) and the role that nerves play in coordinating their activities has been a subject of controversy. We used fluorescent video imaging techniques to study the origin and propagation of excitability simultaneously in LM and CM of the small intestine. **Methods:** Opened segments of guinea pig ileum were loaded with the  $\text{Ca}^{2+}$  indicator fluo-3. Mucosal reflexes were elicited by lightly depressing the mucosa with a sponge. **Results:** Spontaneous  $\text{Ca}^{2+}$  waves occurred frequently in LM ( $1.2 \text{ s}^{-1}$ ) and less frequently in CM ( $3.2 \text{ min}^{-1}$ ). They originated from discrete pacing sites and propagated at rates 8–9 times faster parallel (LM, 87 mm/s; CM, 77 mm/s) compared with transverse to the long axis of muscle fibers. The presence of  $\text{Ca}^{2+}$  waves in one muscle layer did not affect the origin, rate of conduction, or range of propagation in the other layer. The extent of propagation was limited by collisions with neighboring waves or recently excited regions. Simultaneous excitation of both muscle layers could be elicited by mucosal stimulation of either ascending or descending reflex pathways. Neural excitation resulted in an increase in the frequency of  $\text{Ca}^{2+}$  waves and induction of new pacing sites without eliciting direct coupling between layers. **Conclusions:** Localized, spontaneous  $\text{Ca}^{2+}$  waves occur independently in both muscle layers, promoting mixing (pendular or segmental) movements, whereas activation of neural reflexes stimulates  $\text{Ca}^{2+}$  waves synchronously in both layers, resulting in strong peristaltic or propulsive movements.

To understand motility patterns in the gastrointestinal tract, it is important to discern how longitudinal (LM) and circular muscles (CM) act together to produce both mixing and peristaltic movements. The 2 muscle layers are innervated by different populations of motor neurons with different distributions,<sup>1–3</sup> suggesting that they can be regulated independently by nerves. Motor neurons to the LM of the small intestine are mainly (~95%) excitatory, whereas those to the CM are both excitatory and inhibitory (with roughly equal contribu-

tions).<sup>3</sup> Movements of either muscle alone should produce mixing of chyme<sup>4</sup>; however, relative movements of the muscle layers and the role that nerves play in coordinating their activities have been a subject of controversy for many years. Recently, Wood<sup>5</sup> argued that the LM and CM layers cannot contract or relax together because “. . . the anatomical arrangement of the circular and longitudinal muscle coats and the laws of geometry dictate that they are antagonistic muscles (i.e., shortening of one opposes shortening of the other).” Bayliss and Starling<sup>6</sup> in 1899 were aware of the possibility of such passive mechanical interactions between the muscles, but considered them to be “negligible” with their recording system, which revealed synchronous contractions and relaxations of the 2 layers during peristalsis in the canine small intestine.

Other studies involving the small intestine have also suggested contrasting views of conduction between muscle layers, including: (1) movements of the 2 layers are synchronous; (2) muscle layers are electrically coupled; (3) movements are 180° out of phase with each other; and (4) there is no correlation between movements of the 2 muscle layers.<sup>7</sup> In canine small intestine, studies have shown that muscles appear to move 180° out of phase with respect to each other, whereas in the stomach they appear to contract together.<sup>8</sup> Melville et al.<sup>9</sup> used video methods to monitor markers along the length of the feline duodenum and concluded that contractions in LM are independent of those in CM. Similar conclusions were reached by Yokoyama and North<sup>10</sup> who found no correlation between spontaneous action potentials in LM and CM of the guinea pig small intestine. At the threshold for peristalsis, however, both muscle layers exhibited bursts of action potentials at the same time, suggesting that activation of neural reflex pathways could coordinate activities.

*Abbreviations used in this paper:* ACh, acetylcholine; CM, circular muscle; ICC, interstitial cells of Cajal; KRB, Krebs–Ringer’s bicarbonate; LM, longitudinal muscle; ROI, region of interest.

© 2000 by the American Gastroenterological Association  
0016-5085/00/\$10.00  
doi:10.1053/gg.2000.7042

Studies of peristalsis using the Trendelenburg preparation also emphasized differences in the movements of the 2 muscle layers of the guinea pig small intestine during propulsion.<sup>11</sup> During peristalsis, there was an initial contraction of LM (type I contraction) that was later followed by a propagating contraction of the CM (type II contraction). During the type II contractions, LM appeared to relax. These studies, as well as others showing that the 2 muscles respond differently to drugs and electrical field stimulation, led Kottogoda<sup>12</sup> to put forth the now widely held notion of reciprocal innervation: when excitatory nerves to one layer are activated to cause contraction, inhibitory nerves to the other layer are activated at the same time to cause relaxation.

Kottogoda's conclusions are, however, based on mechanical studies that sometimes fail to eliminate possible passive mechanical interactions between the 2 muscle layers. Contraction of the CM may lead to passive lengthening of the LM and vice versa.<sup>6,13,14</sup> Recent studies, which have focused on designs to avoid these interactions, have shown that in response to peristaltic waves, point activation of enteric reflexes, and extrinsic nerve stimulation, both muscle layers in the small and large intestine contract and relax together,<sup>14-20</sup> as originally suggested by Bayliss and Starling.<sup>6</sup> In addition, recent less invasive techniques such as video imaging (guinea pig small intestine)<sup>21</sup> and ultrasonography (human esophagus)<sup>22</sup> have also shown synchronous contraction and relaxation of the 2 muscle layers after activation of enteric reflexes, suggesting that excitatory and inhibitory motor neurons to both layers can be activated at the same time. Although Hennig et al.<sup>21</sup> found that the 2 muscle layers contracted together during the initial phase of peristaltic contractions, they also observed a lengthening of the intestine when CM contraction became lumenally occlusive.

Electrophysiological studies have generally suggested that slow waves and their associated contractions occur synchronously in both muscle layers of the intestine.<sup>23-25</sup> This was thought to occur because slow waves generated in the LM spread electrotonically into the CM via bridges of muscle cells spanning the 2 layers.<sup>23</sup> Although muscle fibers have been observed to occasionally bridge the 2 muscle layers,<sup>26</sup> there seems to be little or no electrotonic coupling<sup>27</sup> or spread of action potentials<sup>10</sup> between the LM and CM in the guinea pig ileum. Recent reports also suggest that indirect coupling may exist because slow waves appear to arise from common networks of pacemaker cells (interstitial cells of Cajal [ICC]) in the vicinity of the myenteric plexus located between the 2 layers.<sup>28</sup>

Calcium is the intracellular mediator linking electrical excitation with muscle contraction. Recently, we introduced low-light video imaging techniques to directly visualize the origin and spread of  $\text{Ca}^{2+}$  waves in the guinea pig large intestine<sup>29</sup> and canine gastric antrum.<sup>30</sup> In this study, we extend these techniques to visualize the propagation of  $\text{Ca}^{2+}$  waves simultaneously in the LM and CM layers of the guinea pig small intestine. We show that  $\text{Ca}^{2+}$  waves occur in both layers, but a wave in 1 layer has no effect on the origin, rate of propagation, or range of spread of waves in the other layer. Neural induction of new pacing sites at the same time in both muscles provides a mechanism for synchronized contraction of the 2 layers during peristalsis.

## Materials and Methods

### Muscle Preparation

Guinea pigs weighing between 250 and 300 g were killed by asphyxiation in a  $\text{CO}_2$  chamber, followed by severing of the carotid arteries and exsanguination, in accordance with the requirements of the Animal Ethics Committee at the University of Nevada, Reno, which follows the National Institutes of Health guidelines (NIH Publication no. 80-23; revised 1978). All efforts were made to minimize suffering of animals and the number of animals used in these experiments. Segments (5–6 cm) of small intestine were removed from the region 10–15 cm above the ileocecal junction. Segments were opened along the mesenteric border and pinned flat across an optical window with the mucosa uppermost to the bottom of a custom-designed organ chamber (Figure 1), as described previously.<sup>1,29,31</sup> A rectangular region ( $1 \times 1$  cm) of mucosa above the optical window was removed to avoid excessive background light from entering the field of view. Tissues were continuously perfused with oxygenated Krebs–Ringer's bicarbonate (KRB) solution for 2–3 hours at  $37^\circ\text{C}$  before dye loading.

### Loading Muscles With Fluorescent Indicator

After equilibration, the area of the tissue with exposed muscle was treated with  $5 \times 10^{-6}$  mol/L of the  $\text{Ca}^{2+}$ -sensitive indicator fluo-3 acetoxymethyl ester, 0.01% dimethyl sulfoxide, and 0.025% of the noncytotoxic detergent cremophor EL for 15–25 minutes. LM and CM in the dissected island lying over the optical window could be loaded independently (or at the same time) with fluo-3 by pipetting the  $\text{Ca}^{2+}$  indicator under the serosal surface to load the LM or onto the submucosal surface to load the CM.<sup>29-32</sup> When dye loading was complete, tissues were again allowed to equilibrate in KRB solution for an additional 15–20 minutes at  $37^\circ\text{C}$  before the experiments.

### Evoked Neural Responses

Ascending or descending neural reflexes were evoked by mechanically stimulating the mucosa 10 mm anal or oral to

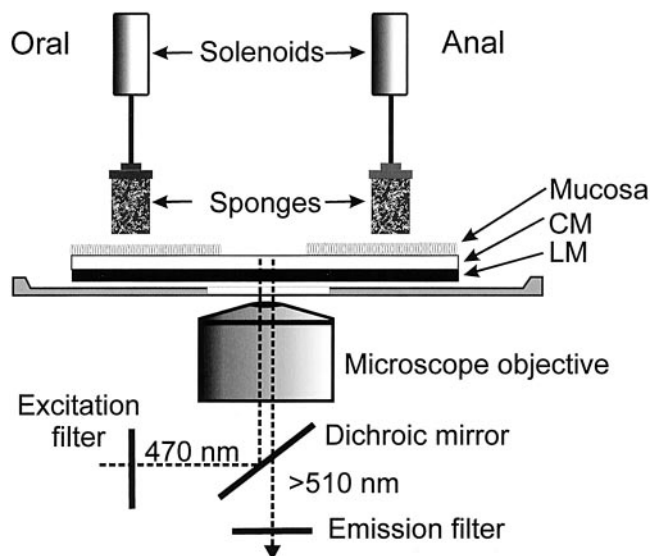


**Figure 1.** Fluorescent imaging and neural stimulation apparatus. The mucosa was removed to create an island of exposed LM and CM situated atop a quartz window positioned over a microscope objective. Ascending or descending neural pathways were evoked by lowering sponges attached to computer-controlled solenoids placed either anally or orally to the recording region, respectively. Tissues within the field of view were irradiated by  $470 \pm 20$  nm light, and fluorescence  $> 510$  nm was collected using an intensified camera.

the recording site, respectively.<sup>1,33,34</sup> Mucosal stimulation was performed using sponges (diameter, 4 mm) that lightly depressed the villi. Sponges were mounted to custom-built, computer-controlled solenoids (Figure 1).<sup>29,34</sup>

### Data Acquisition and Analysis

Muscles were illuminated at  $470 \pm 20$  nm, and fluorescent emissions  $> 510$  nm (e.g., Figure 2A) were recorded as a relative measure of intracellular  $\text{Ca}^{2+}$  concentration ( $[\text{Ca}^{2+}]_i$ ) using an intensified charge-coupled device camera (Dage-MTI model SIT-66X, Michigan City, IN) attached to the videoport of an inverted epifluorescence microscope (Nikon Diaphot, Tokyo, Japan).<sup>31</sup> Usually, a  $10\times$  fluor objective (Nikon) was used, yielding a field of view of  $1.2 \times 1.0$  mm. To compute conduction velocities in the long axis of muscle fibers, a  $2\times$  objective and low-power (e.g.,  $1.6\times$ ) relay lens were sometimes used ( $6.0 \times 5.0$ -mm field of view). Images were stored on a computer-controlled videocassette recorder (Sanyo model GVR-S950, Itasca, IL) at a rate of 30 frames per second.

### Image Analysis

Analysis of videofluorescent signals was performed using both custom-designed and commercially available software (Adobe PhotoShop, San Jose, CA). Images were digitized ( $640 \times 480$  pixels) using a frame grabber (Data Translation model 3152, Marlboro, MA).<sup>31</sup> Because each frame could be analyzed individually using the videocassette recorder, a temporal sampling rate of 30 frames per second could be achieved.

To view propagation, series of contrast-enhanced images

were computed by storing an initial frame (with no apparent activity) as a "background image" (first frame in Figures 3–8). This image was then subtracted from each subsequent frame. To further aid visualization, all contrast-enhanced frames are displayed as "negative images," in which dark areas correspond to regions of increased fluorescent intensity. Conduction velocities were measured by determining the distance traveled by a wave front over a single digitized frame (i.e., over a 33.3-millisecond interval).

To monitor  $\text{Ca}^{2+}$  transients over prolonged periods, regions of interest (ROIs) in the shape of a parallelogram (usually rectangular) were selected (Figure 2A) with elongated sides aligned to the long axis of muscle fibers in each muscle layer (or layers). In some cases, muscle fibers were not precisely orthogonal to each other and sampling parallelograms were constructed at appropriate angles<sup>31</sup> (Figures 7 and 8). Pixel intensities for each ROI were summed and normalized for area (Figure 2B). To determine temporal relationship between activities in different ROIs, event time plots were constructed by thresholding summed intensities and representing each  $\text{Ca}^{2+}$  transient as a vertical line segment (Figure 2C). All event time plots were verified by manually viewing video data on a frame-by-frame basis.

Statistics are reported as mean  $\pm$  SD. All image series in Figures 3–8 are incremented in time from left to right and top to bottom. In addition, all frames are orientated so that the vertical direction is aligned (approximately) with the long axis of LM fibers (oral to anal) and the horizontal direction represents the long axis of CM fibers (as illustrated in Figure 2A).

### Solutions

The KRB used in this study contained (in mmol/L) NaCl, 120.4; KCl, 5.9;  $\text{CaCl}_2$ , 2.5;  $\text{MgCl}_2$ , 1.2;  $\text{NaHCO}_3$ , 15.5;  $\text{NaH}_2\text{PO}_4$ , 1.2; and dextrose, 11.5 (Fisher Scientific, Pittsburgh, PA). This solution had a pH of 7.3–7.4 at  $37.5^\circ\text{C}$  when bubbled to equilibrium with 97%  $\text{O}_2$ –3%  $\text{CO}_2$ . Fluo-3 was purchased from Molecular Probes (Eugene, OR). Dimethyl sulfoxide, atropine, nicardipine, tetrodotoxin, and cremophor EL were obtained from Sigma Chemical Co. (St. Louis, MO).

### Results

By monitoring fluorescent intensities of the indicator fluo-3,  $\text{Ca}^{2+}$  waves could be observed in LM only (serosal loading), in CM only (submucosal loading), or at the same time in both muscle layers (see Materials and Methods and Figure 2).  $\text{Ca}^{2+}$  waves in either muscle layer were completely eliminated by the L-type  $\text{Ca}^{2+}$  channel antagonist nicardipine (1 mmol/L;  $n = 6$ ).

### Origin and Spread of Excitability in LM

Spontaneous  $\text{Ca}^{2+}$  waves (frequency,  $1.2 \pm 0.5/\text{s}$ ;  $n = 14$  tissues) emerged from discrete sites and propagated with anisotropic conduction velocities through the

LM layer of the ileum (Figure 3A). These events were similar to those we observed in LM of the distal colon.<sup>29</sup> Propagation velocities were approximately 8 times faster parallel (87.3 ± 22 mm/s; vertical direction in the field

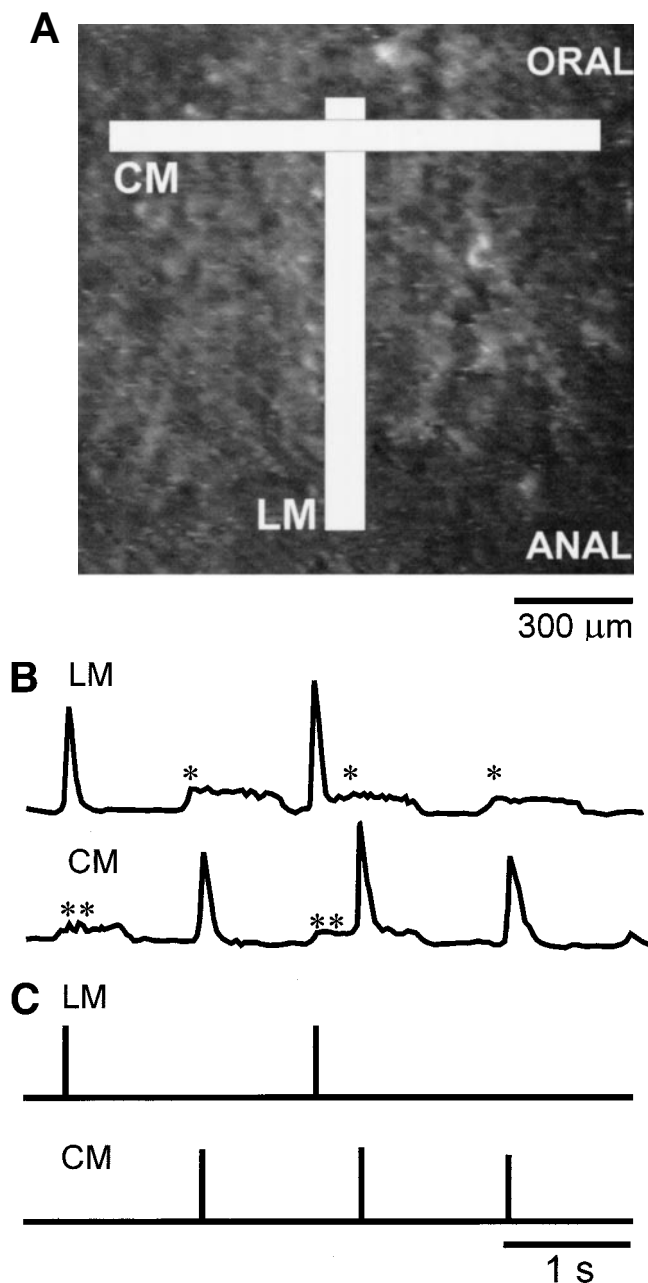


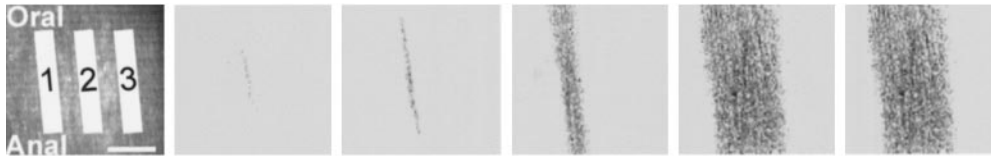
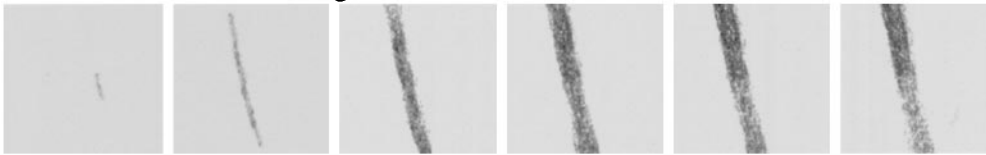
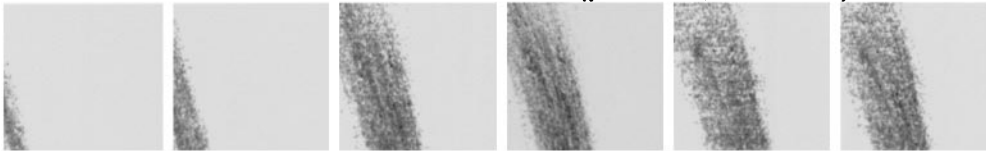
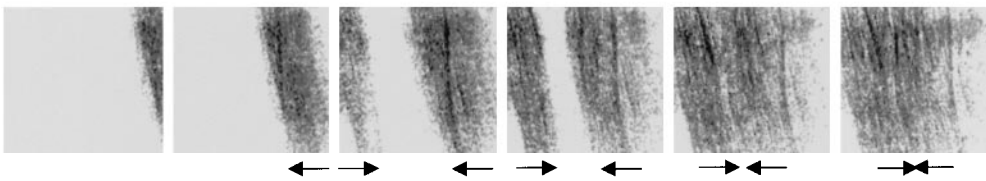
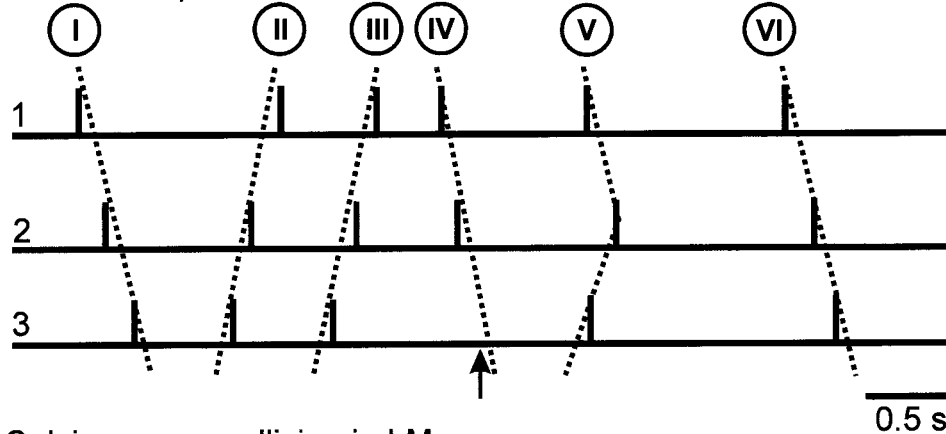
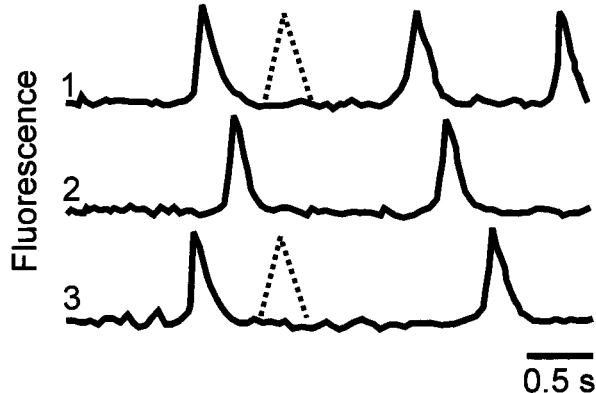
**Figure 2.** Imaging processing steps used to generate event time plots over extended periods. (A) In the background fluorescent image, rectangular ROIs (white rectangles) within the field of view ( $1.2 \times 1.0$  mm) were selected to favor the detection of  $\text{Ca}^{2+}$  transients within LM (long axis of muscle fibers oriented vertically) or CM (long axis of muscle fibers oriented horizontally). (B) Summed pixel intensities from each ROI were normalized for area. Large peaks indicate the spread of  $\text{Ca}^{2+}$  waves in LM (upper trace) and CM (lower trace), whereas smaller peaks in the upper (\*) and lower (\*\*) traces result from  $\text{Ca}^{2+}$  transients sweeping through portions of ROIs in the opposing layer. (C) An amplitude threshold to detect the larger peaks was used to construct event time plots for each muscle layer.

of view of Figure 3A;  $n = 50$  events from 4 tissues) compared with orthogonal ( $10.8 \pm 4.0$  mm/s;  $n = 50$  events from 14 tissues) to the long axis of the LM fibers (Figure 3A). Spontaneous  $\text{Ca}^{2+}$  waves within the LM layer emerged from discrete sites within fields of view (Figure 3A–D) and typically spread outside the field of view.  $\text{Ca}^{2+}$  waves entered the field of view with no preference from the oral, anal, or circumferential directions (Figure 3E). Five percent of  $\text{Ca}^{2+}$  waves (3 of 60 events in 5 tissues) emerged from discrete sites and could be seen to initially spread rapidly along the length of fibers, but failed to propagate for any significant distance orthogonal to the long axis of LM fibers (Figure 3B). These “minimum conducting bundles” were  $250 \pm 85$  μm ( $n = 30$  events from 5 tissues; range, 110–400 μm) in width.

The extent of propagation of  $\text{Ca}^{2+}$  waves in the circumferential axis was limited by encountering refractory or suppressed regions, occasionally for no apparent reason (Figure 3C and E, wave IV), or by colliding with other  $\text{Ca}^{2+}$  waves from neighboring regions (Figure 3D and E, wave V). When opposing  $\text{Ca}^{2+}$  waves collided, they did not propagate past each other (Figure 3D, frames 5 and 6; 3E, wave V; and 3F, dashed lines), suggesting that each wave is followed by a wake of refractoriness. Each collision resulted in the annihilation of a pair of propagating wave fronts parallel to the long axis of muscle fibers (without affecting the wave fronts associated with each event propagating in opposite directions).

$\text{Ca}^{2+}$  waves typically propagated  $11.6 \pm 4.5$  mm ( $n = 50$  events from 4 tissues) in the long axis of LM fibers and terminated by encountering refractory regions or by colliding with other  $\text{Ca}^{2+}$  waves. Termination in this axis resulted in excited regions with thin, finger-like projections (Figure 4A). The locations of these finger-like projections were dynamic, generally changing from event to event.

$\text{Ca}^{2+}$  waves propagating in the long axis of LM fibers were also frequently observed to propagate collaterally around recently excited (i.e., refractory) regions. Figure 4B shows an example of how pathways of  $\text{Ca}^{2+}$  waves can be influenced by the presence of a refractory region. A  $\text{Ca}^{2+}$  wave propagated anally through the center of the field of view (frames 1–6), leaving this area transiently refractory. A second  $\text{Ca}^{2+}$  wave emerged just to the left of the field of view and propagated adjacent to, but not into, the refractory region (frames 8–10). This wave swept around the refractory region, reentering the lower portion of the field of view (frames 10–15) and propagating alongside the region. After a delay, reexcitation of the region initially left refractory by the first wave eventually occurred by circumferential spread inward from adjacent

**A. Emergence and propagation of calcium wave in LM****B. Minimum conducting bundle in LM****C. Termination of calcium wave in LM (panel E, wave IV)****D. Collision between 2 calcium waves in LM (panel E, wave V)****E. Event time plots for 3 ROIs in leftmost frame of panel A****F. Calcium wave collision in LM**

**Figure 3.** Propagation of  $\text{Ca}^{2+}$  waves in LM. (A) The leftmost frame shows background fluorescence of LM. The subsequent sequence (frames 2–6, 0–133 milliseconds) shows the emergence and anisotropic propagation of a  $\text{Ca}^{2+}$  wave. Note that the wave propagates rapidly (leaving the field of view by frame 3) in the direction of the LM fibers (vertical) and less rapidly orthogonal to the long axis of the muscle fibers (horizontal or circumferential direction). Bar = 300  $\mu\text{m}$ . (B) Propagation was rapid in the direction of LM fibers (vertical) but was limited to  $\sim 200 \mu\text{m}$  in the circumferential axis. Occasionally propagation orthogonal to LM fibers stopped for no apparent reason (C and E, wave IV; arrow indicating lack of conduction). In most cases, propagation orthogonal to LM fibers stopped on collision with  $\text{Ca}^{2+}$  waves propagating from the opposite direction (D and E, wave V). Event time plots (E, using 3 ROIs of background image in A) show propagation from both circumferential directions (left-to-right waves I and VI; right-to-left waves II and III). (F) Summed fluorescent intensities during a collision of circumferentially propagating  $\text{Ca}^{2+}$  waves in which the superimposed dashed wave forms indicate the position of  $\text{Ca}^{2+}$  waves if they had propagated through each other with a constant conduction velocity.

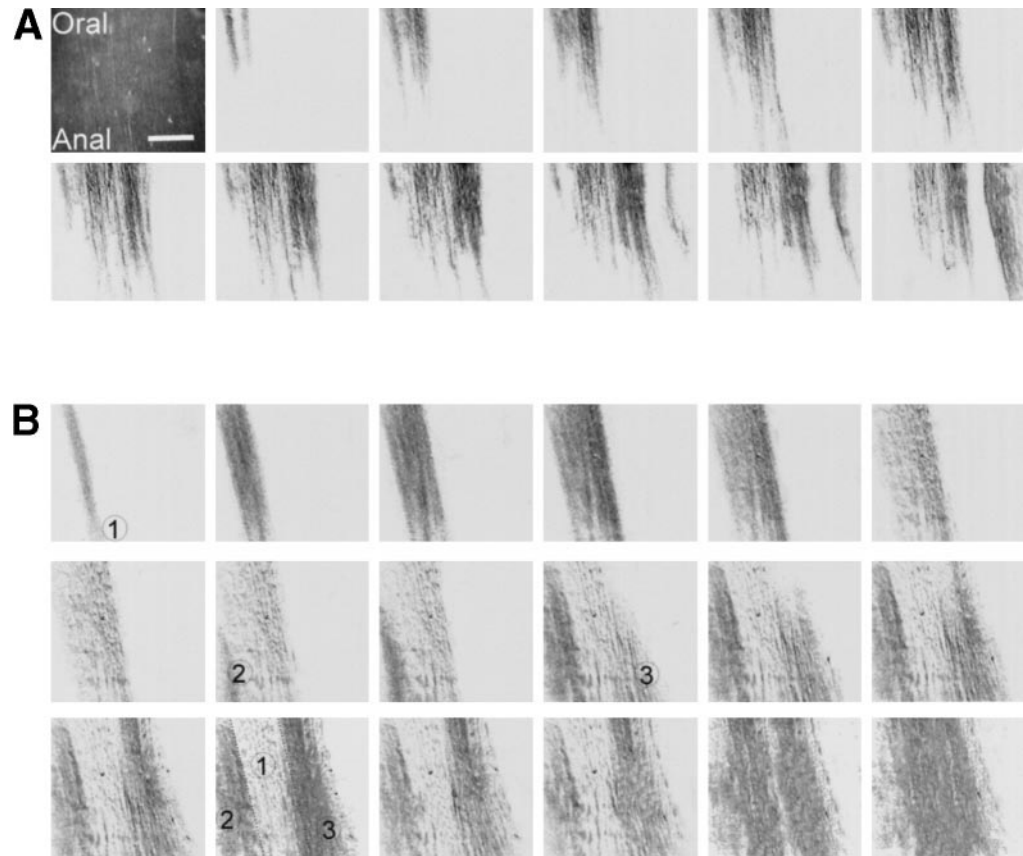


**Figure 4.** Termination of  $\text{Ca}^{2+}$  waves in LM. (A) Frames 2–12 (0–333 milliseconds) illustrate termination of an LM  $\text{Ca}^{2+}$  wave that results in numerous “finger-like” projections in the direction of the long axis of LM fibers. Bar = 300  $\mu\text{m}$ . (B) Initial frames 1–6 (0–166 milliseconds) show an LM  $\text{Ca}^{2+}$  wave that stopped propagating in circumferential directions near the center of the field of view (region labeled 1). A second  $\text{Ca}^{2+}$  wave (initiated in region labeled 2 in frame 8) propagated collaterally around this recently excited region. Frame 14 (with dotted lines at the locations of wave fronts added for clarity) shows that regions 2 and 3 are excited, whereas region 1 is not. After a prolonged delay, the second wave finally enveloped region 1 (frames 17 and 18).

excited regions (frames 15–18). Extremely complex patterns of excitation can arise rapidly as a result of spread around refractory regions.

#### Origin and Spread of Excitability in CM

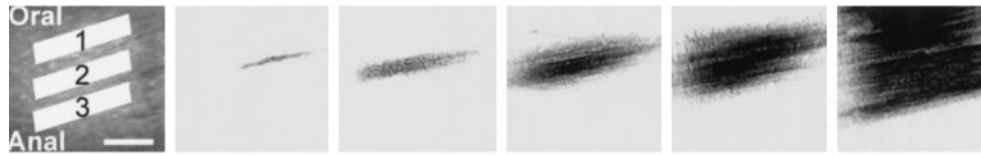
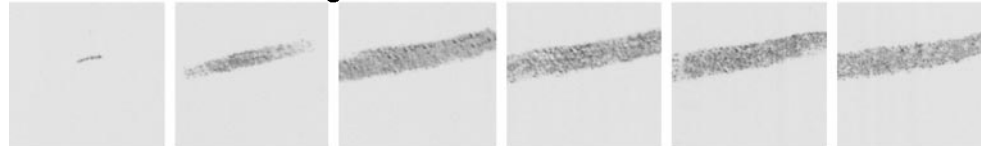
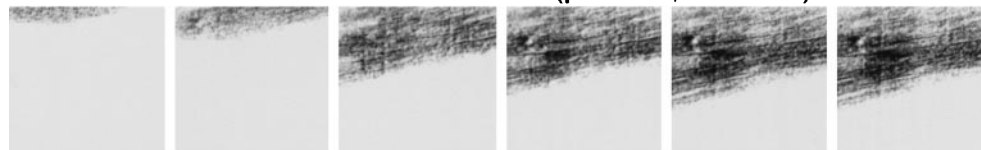
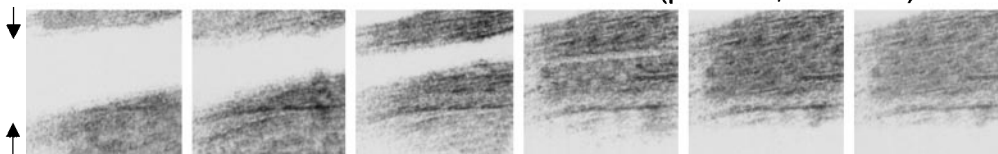
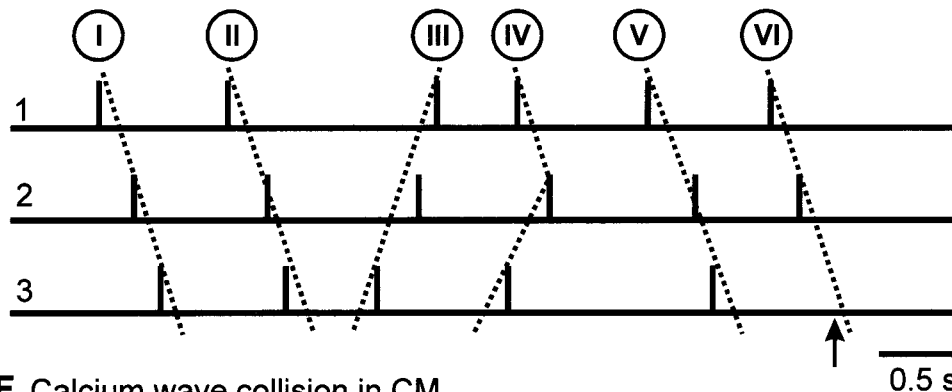
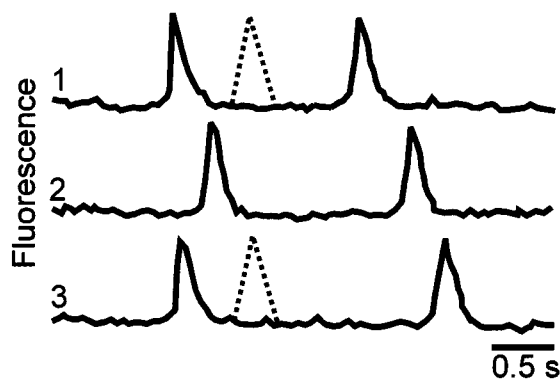
Spontaneous  $\text{Ca}^{2+}$  waves ( $3.2 \pm 0.2$  events/min;  $n = 14$  tissues) were observed much less frequently in CM compared with longitudinal tissue. The relative absence of  $\text{Ca}^{2+}$  waves in CM was not caused by insufficient loading of the muscle with fluo-3, because after a period of mucosal stimulation, there was a marked increase in the density and frequency of observed  $\text{Ca}^{2+}$  waves (see below). In some preparations in which both layers were loaded with fluo-3 (3 of 50 events in 4 tissues), it was possible to study the activity in CM during lulls in the almost continual activity of the longitudinal layer.  $\text{Ca}^{2+}$  waves within the CM layer exhibited many of the same characteristics as those seen in LM. They were observed to emerge repeatedly from discrete sites and propagate anisotropically (Figure 5A). Propagation velocities were approximately 9 times faster parallel ( $77.7 \pm 13.5$  mm/s; 50 events in 4 tissues) than orthogonal ( $8.4 \pm 1.8$  mm/s; 100 events from 14 tissues) to the long axis of CM fibers. Infrequently (2 events of 50 from 4 tissues),  $\text{Ca}^{2+}$  waves emerged from discrete sites and propagated rapidly in the long axis but failed to

spread very far in the short axis of the CM fibers. This resulted in narrow bands (i.e., “minimum conducting bundles”) of muscle excitation ( $200 \pm 20$   $\mu\text{m}$ ;  $n = 30$  events from 5 tissues; range, 150–300  $\mu\text{m}$ ) that extended across the width of the field of view (Figure 5B).  $\text{Ca}^{2+}$  waves entered the field of view with no directional preference (e.g., Figure 5E, waves I, II, III, and V), but sometimes ceased to propagate through the field of view (Figure 5C and E, wave VI) for no apparent reason.

The extent that a  $\text{Ca}^{2+}$  wave traveled along the bowel (slow axis) was generally limited by collisions (Figure 5D and E, wave IV). Colliding  $\text{Ca}^{2+}$  waves in the CM did not propagate past each other (Figure 5E, wave IV; and Figure 5F) and (as in LM) terminated in a single event of similar magnitude to the waves before the collision (Figure 5F).  $\text{Ca}^{2+}$  wave propagation in the long axis of the CM fibers resulted in an entire excited band of muscle that invariably encompassed the entire width ( $5.3 \pm 1.2$  mm) of the preparation, spreading as a planar wave front anally, orally, or (most frequently) in both directions.

#### Activities in Both LM and CM Layers

By adjusting the focal plane of the microscope, we were able to visualize muscle fibers and  $\text{Ca}^{2+}$  waves in both muscle layers at the same time, thereby monitoring the excitability in LM and CM simultaneously. A typical

**A. Emergence and propagation of calcium wave in CM****B. Minimum conducting bundle in CM****C. Termination of calcium wave in CM (panel E, wave VI)****D. Collision between 2 calcium waves in CM (panel E, wave IV)****E. Event time plots for 3 ROIs in leftmost frame of panel A****F. Calcium wave collision in CM**

**Figure 5.** Propagation of  $\text{Ca}^{2+}$  waves in CM. (A) Frames 2–6 (0–133 milliseconds) show the emergence and anisotropic propagation of a  $\text{Ca}^{2+}$  wave in CM with rapid conduction in the long axis of CM fibers (horizontal) and slower conduction along the length of the intestine (vertical). Bar = 300  $\mu\text{m}$ . (B) A  $\text{Ca}^{2+}$  wave emerged (frame 1) in CM and propagated rapidly in frames 1–3 (0–66 milliseconds) across the field of view but failed to propagate in frames 4–6 (100–166 milliseconds) along the length of the intestine (limited to  $\sim 250$   $\mu\text{m}$ ). (C) As illustrated in frames 1–6 (0–166 milliseconds), occasionally propagation orthogonal to CM fibers stopped for no apparent reason (E, wave VI; arrow indicating lack of conduction). (D) As shown in frames 1–6 (0–166 milliseconds), in most cases propagation in CM along the intestine stopped upon collision with another  $\text{Ca}^{2+}$  wave (see frames 3–6; E, wave IV, and F). (E) Event time plots (using 3 ROIs shown in the background image in A) show propagation from either direction along the gut (oral to anal, waves I, II, V, and VI; anal to oral, wave III). (F) Summed fluorescent intensities during a collision of anally and orally propagating  $\text{Ca}^{2+}$  waves in CM in which superimposed dashed wave forms indicate the position of  $\text{Ca}^{2+}$  waves if they had propagated through each other with a constant velocity.

**Figure 6.**  $Ca^{2+}$  waves recorded simultaneously in both layers.  $Ca^{2+}$  waves were viewed in both LM (long axis of LM fibers oriented vertically) and overlying CM (long axis of CM fibers oriented horizontally). Arrows indicate the direction of propagation of  $Ca^{2+}$  waves in the slow axes of LM and CM. (A) An established  $Ca^{2+}$  wave within the LM (first frame) did not affect the ability of  $Ca^{2+}$  waves to propagate in CM (frames 2–12; 33–333 milliseconds). Bar = 300  $\mu m$ . (B) Conversely, a  $Ca^{2+}$  wave established within the CM (frames 1–6; 0–166 milliseconds) did not obstruct the propagation of a  $Ca^{2+}$  wave in the underlying LM (frames 7–12; 199–366 milliseconds).

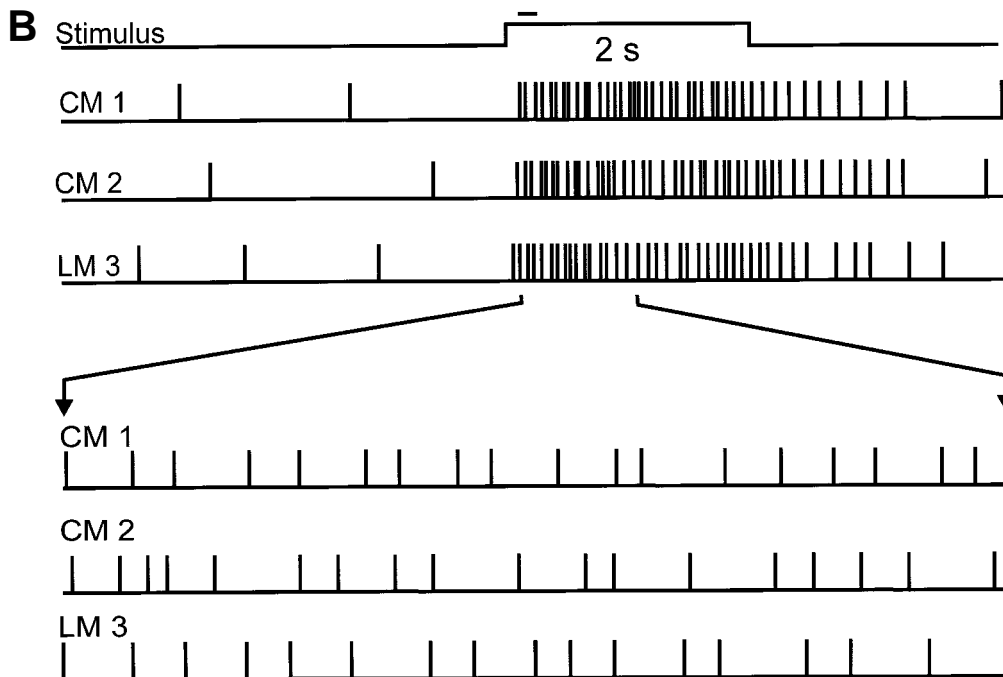
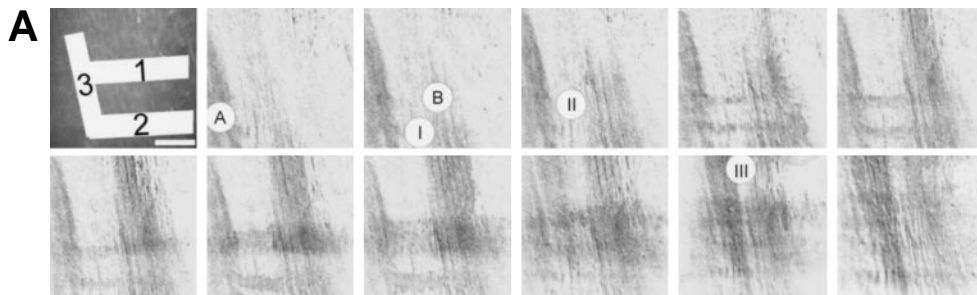
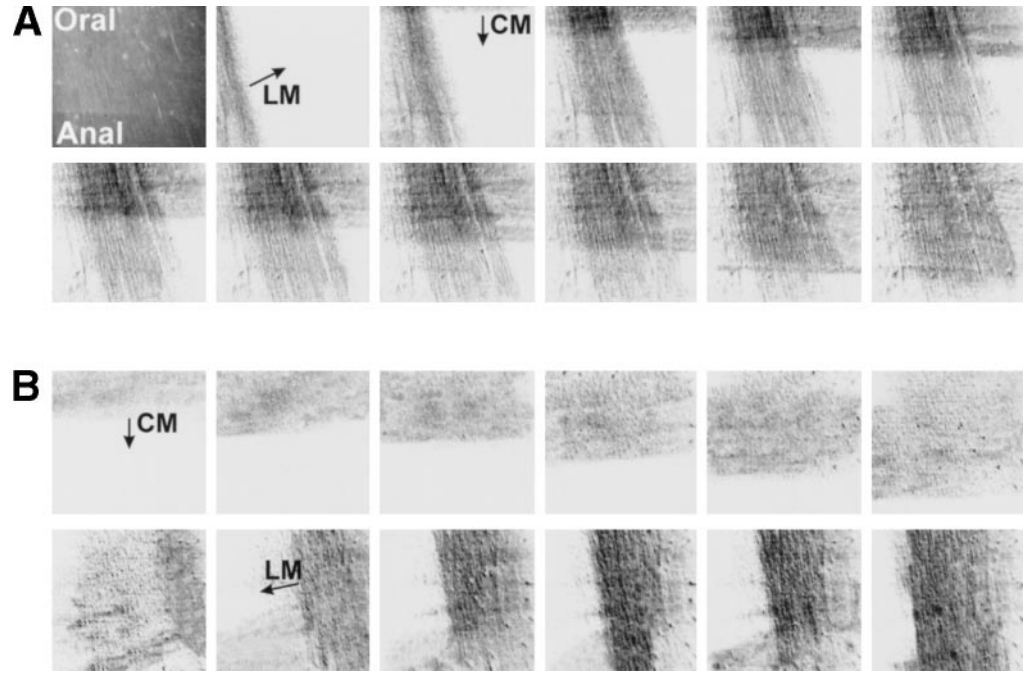


**Figure 7.** Ascending excitatory reflex. (A) Frames 2–12 (0–333 milliseconds) show the induction of multiple pacing sites in LM (labeled A and B) and CM (labeled I–III) in response to depression of the mucosa 10 mm anal to the recording site. Bar = 300  $\mu m$ . (B) The upper trace shows a time line of the application of the stimulus, and the bar above the stimulus trace shows the time over which frames in A were recorded. Event time plots were constructed based on intensities in CM (CM 1 and CM 2) and LM (LM 1) from the 3 ROIs in the background image in A. Stimulation elicited new pacing sites in both muscle layers and increased overall  $Ca^{2+}$  wave frequency (ascending excitation). An expanded time scale during stimulation shows that some events in CM did not propagate throughout the field of view and individual events in LM do not coincide with activity in the CM.

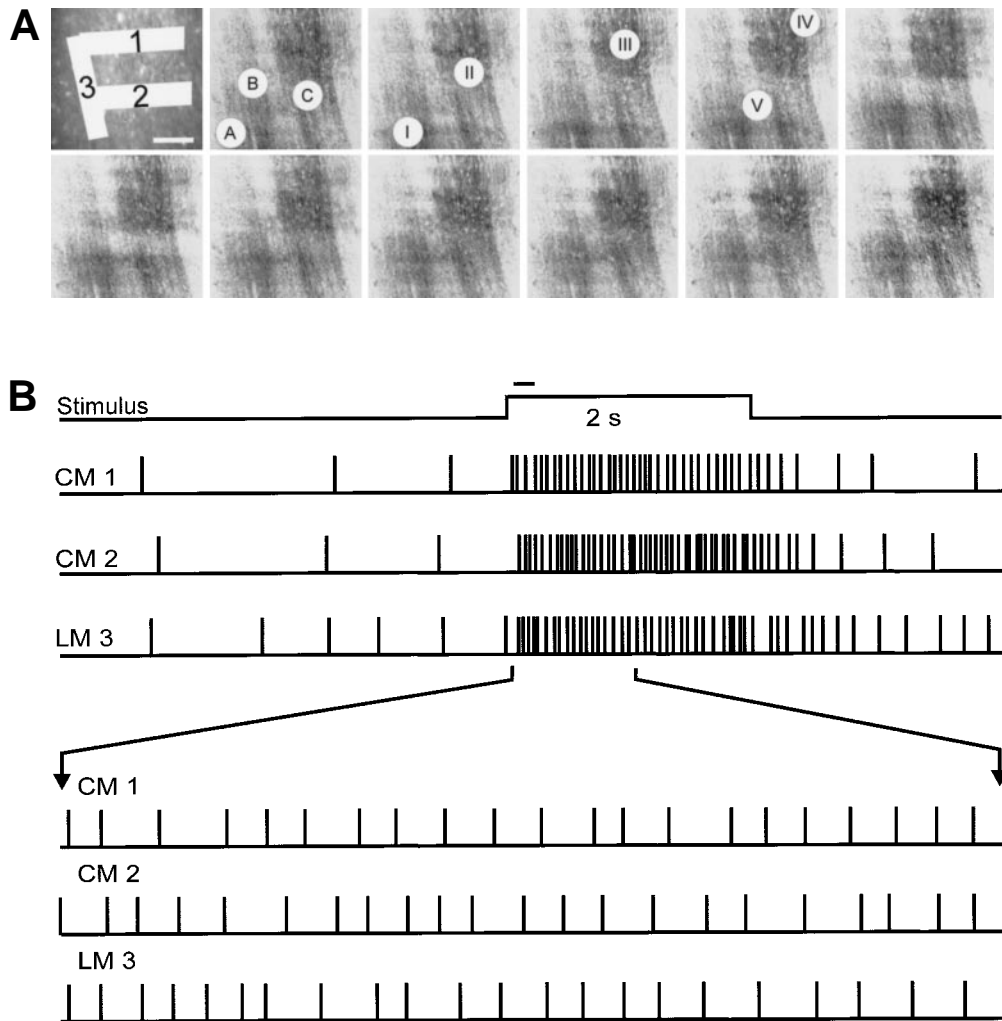


**Figure 8.** Descending excitatory reflex. (A) Frames 2–12 (0–333 milliseconds) show the induction of multiple pacing sites in LM (labeled A–C) and CM (labeled I–V) in response to depressing the mucosa 10 mm oral to the recording site. Bar = 300  $\mu$ m. (B) The upper trace shows a time line of the application of the stimulus, and the bar above the stimulus trace shows the time over which frames in A were recorded. Event time plots were constructed based on intensities in CM (CM 1 and CM 2) and LM (LM 1) from the 3 ROIs in the background image in A. New pacing sites in both muscle layers and increases in overall pacing frequency (descending excitation) were elicited by mucosal stimulation. The expanded time scale during stimulation shows that some events in CM did not propagate throughout the field of view, and activity in LM is not coupled with events in CM.

example of the simultaneous propagation of  $\text{Ca}^{2+}$  waves in both muscle layers is shown in Figure 6. In Figure 6A, a  $\text{Ca}^{2+}$  wave in the LM entered the field of view from the left and propagated circumferentially (frames 2–12) across the field of view. Then a  $\text{Ca}^{2+}$  wave in the CM spread with a similar conduction velocity in an oral-to-anal direction, passing over without disturbing the wave in the LM (frames 3–12). As the waves overlapped, light intensity increased above levels generated by a  $\text{Ca}^{2+}$  wave within a single muscle layer. This arose as a result of the camera summing fluorescence from the 2 muscle layers and not because of increased intracellular  $[\text{Ca}^{2+}]$  in these regions.

Figure 6A shows that the spread of a  $\text{Ca}^{2+}$  wave in LM does not affect propagation in the circular layer. The series of frames in Figure 6B show the opposite sequence of activities in the same tissue. The trail of refractoriness left by a  $\text{Ca}^{2+}$  wave in the CM layer propagating orally across the field of view (frames 1–7) did not affect the emergence or circumferential spread of a  $\text{Ca}^{2+}$  wave in the underlying LM layer (frames 7–12). Spontaneous  $\text{Ca}^{2+}$

waves in both muscles were blocked by atropine (1 mmol/L; 5 tissues), suggesting they are induced by cholinergic activity.

#### Neurally Induced Excitation of CM and LM Layers

As we have shown recently,<sup>20</sup> mucosal stimulation of the ileum produces synchronous contractions of both LM and CM layers both above (ascending excitation) and below (descending excitation) the site of stimulation. Experiments were performed to determine if activation of excitatory reflex pathways affects the spread of  $\text{Ca}^{2+}$  waves within and between each muscle layer.

Mechanical stimulation of the mucosa increased the frequency of  $\text{Ca}^{2+}$  waves both oral (ascending excitation: LM from  $1.7 \pm 0.8$  to  $11.9 \pm 3.1$   $\text{s}^{-1}$  and CM from  $0.07 \pm 0.01$  to  $12.8 \pm 2.8$   $\text{s}^{-1}$ ; 5 responses from 5 tissues) and anal (descending excitation: LM from  $1.4 \pm 0.6$  to  $13.4 \pm 2.6$   $\text{s}^{-1}$  and CM from  $0.06 \pm 0.01$  to  $13.9 \pm 3.0$   $\text{s}^{-1}$ ; 5 responses from 5 tissues) to the stimulus. Events were initiated from multiple pacing

sites, at the same time in both muscle layers (Figures 7 and 8). The neurally evoked increase in the number of pacing sites seems to be the basis for both ascending and descending excitation.<sup>1,16,19,20,34,35</sup> Exploded views of event traces illustrate that during stimulation of neural reflexes, there was a reduced temporal correlation of  $\text{Ca}^{2+}$  waves induced across the CM (Figure 7B, CM 1 vs. CM 2; Figure 8B, CM 1 vs. CM 2) and no correlation between waves induced in CM with those induced in LM (Figure 7B, CM 1 and CM 2 vs. LM 3; Figure 8B, CM 1 and CM 2 vs. LM 3).

Reflexly induced increases in the frequency of  $\text{Ca}^{2+}$  waves in both the LM and CM layers were abolished by atropine (1 mmol/L) and tetrodotoxin (1 mmol/L).

## Discussion

Motility patterns in the gastrointestinal tract are primarily coordinated by slow waves initiated in ICC that appear to spread electrotonically into underlying smooth muscle cells where they can generate  $\text{Ca}^{2+}$ -dependent action potentials,<sup>28,36,37</sup> and by the activation of intrinsic and extrinsic nerves that regulate these activities.<sup>15,19</sup> Action potential firing in smooth muscles triggers  $\text{Ca}^{2+}$  influx, which is the primary activator of muscular contraction.<sup>28</sup>

Using fluorescent imaging techniques, we have been able to observe elevations in intracellular  $[\text{Ca}^{2+}]$  that propagate in both LM and CM layers of the guinea pig small intestine. These  $\text{Ca}^{2+}$  waves depend on spontaneous release of acetylcholine (ACh) from cholinergic motor neurons because they are blocked by atropine (which also suggests some degree of cholinergic tone).<sup>20</sup>

Spontaneous  $\text{Ca}^{2+}$  waves are more frequent in LM than in CM. They are eliminated by nifedipine (L-type channel blocker) and are therefore likely to be initiated by smooth muscle action potentials,<sup>28,38</sup> which, like local contractions,<sup>9,21,39</sup> are more frequent in LM than in CM.<sup>10,25</sup> The action potential dependence of  $\text{Ca}^{2+}$  waves is also supported by the observation that they propagate along the long axis of muscle fibers with conduction velocities that are similar to velocities (67–88 mm/s) of action potentials along strips of guinea pig taenia coli.<sup>40</sup>

It is generally considered that in most smooth muscle tissues, action potentials are initiated by slow waves. However, classical slow waves are rare in open-sheet preparations of guinea pig ileum, presumably because cutting the preparation may lead to a lack of entrainment between pacemaking cells (presumably ICC).<sup>41</sup> Action potentials in these opened-sheet preparations are likely initiated by fluctuations in membrane potential caused by the random coupling of slow wave generators. This

coupling may be enhanced by ACh, which increases the frequency and amplitude of slow waves.<sup>32,42</sup> Alternatively, action potentials could be produced by ACh acting directly on muscles, which can also generate oscillations in membrane potential similar to slow waves.<sup>43</sup> The maximal extent of propagation of action potentials is determined by the area of muscle depolarized by the slow wave and limited temporally by the repolarization phase of the slow wave.<sup>44</sup>

Spontaneous  $\text{Ca}^{2+}$  waves in LM exhibit characteristics similar to those we recently reported in LM of the distal colon.<sup>29</sup> The constant shifting in pacing sites, which is especially characteristic of LM, probably prevents exposure of cells to sustained high levels of intracellular  $\text{Ca}^{2+}$ , which may be toxic to individual muscle cells.<sup>45,46</sup> Overall, the shifting pacing sites can maintain a basal level of contractile activity at the tissue level.

## Spread of Excitability

Propagation velocities of  $\text{Ca}^{2+}$  waves are similar and show a similar anisotropy with respect to orientation of muscle fibers within LM and CM. In both layers, waves are 8–9 times faster parallel compared with perpendicular to the long axis of muscle fibers (Figures 3 and 5). This anisotropy in the conduction velocities of  $\text{Ca}^{2+}$  waves likely reflects the difference in electrotonic coupling parallel and transverse to each muscle fiber<sup>38</sup> which, in turn, is a determinant of action potential velocity in the 2 axes.

Conduction in each axis of LM should produce complex shearing forces that stir chyme by generating local regions of rapid wall shortening. These regions spread more slowly in the circumferential direction until they collide with adjacent  $\text{Ca}^{2+}$  waves (Figure 3). Spontaneous local contraction of LM on one side of the intestinal tube results in a decrease in the radius of curvature on that side of the lumen. During contraction, chyme is bidirectionally displaced relative to the inner wall of the lumen, exposing the contents to new regions of mucosa, which in turn promotes mixing and absorption. These asymmetric contractions of LM produced by local, anisotropically propagating  $\text{Ca}^{2+}$  waves may contribute to the “squirming” motion (Figure 9A) of the small intestine commonly observed *in vivo* and *in situ*.

In contrast, anisotropic propagation velocities of  $\text{Ca}^{2+}$  waves in CM allow for rapid conduction around the circumference of the intestine. This should organize excitability of this layer into rings of contraction (Figure 4) that propagate slowly in the short axis of CM fibers (along the gut) until they encounter another recently excited region. These slowly conducting rings of contrac-

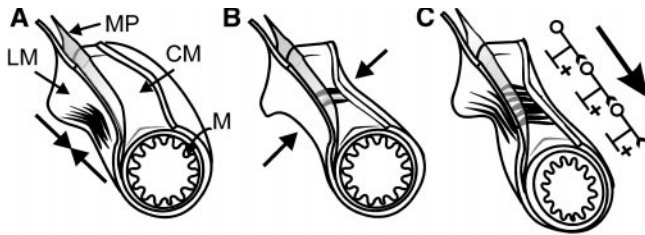


**Figure 9.** Patterns of force development in the ileum. (A) Spontaneous  $\text{Ca}^{2+}$  waves in LM generate a radially asymmetric force about the lumen resulting in a "squirming" motion. (B) Spontaneous  $\text{Ca}^{2+}$  waves in CM produce ring-like contractions of the lumen resulting in a "squeezing" motion. In both cases, propagation of  $\text{Ca}^{2+}$  waves is governed primarily by the properties of the syncytium. (C) Upon neural stimulation, new pacing sites are induced in both muscle layers during peristalsis. The overall spread of this region of increased  $\text{Ca}^{2+}$  wave density is governed by the spread of excitability in the enteric nervous system.

tion produce a "squeezing" of the lumen (Figure 9B) to promote additional mixing and absorption.

### Minimum Motor Units

In both layers there seems to be a minimum width of muscle that can support the spread of  $\text{Ca}^{2+}$  transients parallel to muscle fibers, but not for a significant distance orthogonal to the long axis of muscle fibers. This width, which is  $\sim 200 \mu\text{m}$  in LM and  $\sim 250 \mu\text{m}$  in CM, is consistent with the concept of a minimum width (motor unit) of parallel smooth muscle fibers necessary to sustain action potential propagation.<sup>48,49</sup> The width of LM motor units is similar to the extent of spread of terminal axons of LM motor neurons,<sup>2</sup> suggesting that these bands of muscle may be directly activated by release of ACh from individual motor neurons. Similarly, the motor unit in CM may be the width of the ring of muscle innervated by the circumferential spread of axonal collaterals from CM motor neurons.

### Extent of Propagation

The extent of propagation varies from the minimum width of muscle that can sustain propagation ("minimum conducting bundle") to complete sweeps across the field of view.  $\text{Ca}^{2+}$  waves originating from any one pacing site in a particular muscle layer are not repeatedly restricted by identifiable structures. Instead, waves can propagate through any neighboring region and around regions of the same layer recently excited and/or in a refractory state. The exact dynamics of  $\text{Ca}^{2+}$  wave termination varied somewhat in each muscle layer. In the long axis of CM fibers, the extent of propagation seems to be limited by the circumference of the lumen.  $\text{Ca}^{2+}$  wave propagation in this axis is rapid and always extended to the edges of a segment. This suggests that in a tube, a wave is only limited by colliding with itself (producing a ring-like constriction). In the short axis of both muscle

layers, the extent of propagation is limited by (1) collisions with neighboring  $\text{Ca}^{2+}$  waves, (2) encountering regions that have recently been excited (i.e., that are refractory), and less often (3) stopping for no apparent reason. In all cases,  $\text{Ca}^{2+}$  wave fronts stop as a plane (a straight line when viewed in 2 dimensions) of excitability.

Parallel to the long axis of longitudinal fibers, events terminated with an uneven profile, generating finger-like projections (Figure 4) resulting from either intermittent branch-point failure of action potentials to cross anastomoses joining muscle bundles<sup>26</sup> or encountering regions that had recently been excited. Wave fronts spread around refractory regions, forming multiple finger-like projections (collateral pathways). Some refractory regions are as small as minimum motor units. When a wave encounters such a region there is often an apparent delay as the  $\text{Ca}^{2+}$  wave takes collateral pathways around the region in the slower axis. Collisions and branch-point failure of action potentials restrict contractions in the long axis of the LM from sweeping the entire length of the intestine, thus maintaining regional regulation of contraction. In addition, these finger-like terminations result in a more gradual transition in excitability between segments of small intestine in the excited state vs. those in a nonexcited state, in turn avoiding cell damage by reducing large strain gradients across the transition zone.

### Independence of the Two Muscle Layers

For sometime there has been controversy over whether the 2 muscle layers can act independently (see introduction). Studies of spontaneous contractions suggest that they can because events occur much more often in LM than in CM.<sup>9,21,39</sup> Action potentials are common in LM to the degree that it is difficult to find a region void of activity for any extended period of time. Local contractions in LM sum to produce the overall pendular or rocking movements that are characteristic of this layer.<sup>6,21,39</sup> In circular tissues of the small intestine,  $\text{Ca}^{2+}$  waves seem to be generated only when slow waves propagating through bulk CM are of sufficient amplitude to depolarize spiking cells in the innermost dense circular region. The combination of slow waves and action potentials may be required for ring-like contraction of CM.<sup>49</sup>

The current study clearly shows that  $\text{Ca}^{2+}$  transients in the LM and CM layers in the guinea pig small intestine are not coupled because  $\text{Ca}^{2+}$  waves occurring in 1 muscle layer do not induce new pacing sites, affect propagation, or stop propagation from occurring in the opposing layer. In addition, although refractoriness limits the extent of propagation in 1 layer, there seems to be no influence of the refractory period on  $\text{Ca}^{2+}$  waves in the other layer.

If  $\text{Ca}^{2+}$  waves could spread from 1 layer to the other, overall wave fronts would not spread in a planar fashion transverse to the long axis of muscle fibers, but would propagate diagonal to the long axis in each layer. The exact direction would depend on the relative magnitude of the fastest velocities in each layer. Because the fastest conduction velocities parallel to the long axis of each muscle layer are similar, the observed direction of propagation would be approximately  $45^\circ$  relative to the long axis in each muscle layer. By maintaining separate activities, tissues are able to maintain greater regional control over excitability. If there were communication between muscle layers, the slower conducting axis would be circumvented by rapid propagation velocities in the other muscle and would not play a role in movement of chyme. In contrast, independent activities in each muscle layer allow the slow-conduction velocities, which are more consistent with viscoelastic properties of chyme, to promote mixing.

#### Effects of Neural Reflexes

Mucosal reflex stimulation increases the number of pacing sites and the frequency of  $\text{Ca}^{2+}$  waves at the same time in LM and CM layers both above (ascending excitation) and below (descending excitation) the site of stimulation. These increases, which mirror the rapid action potential firing of muscles during peristalsis,<sup>10,50</sup> suggest they are the basis for synchronous reflex contractions of LM and CM layers observed both oral (ascending) and anal (descending excitation) to mucosal stimuli.<sup>20</sup>

In the guinea pig distal colon, a similar induction of new pacing sites occurs in LM oral to the stimulus, although anal to the stimulus  $\text{Ca}^{2+}$  waves were completely blocked while the mucosa was depressed.<sup>29</sup> This descending inhibition is followed by excitation or induction of new pacing sites ("off excitation") after the termination of the stimulus.<sup>29</sup> The suppression of  $\text{Ca}^{2+}$  waves seems to underlie the nitric oxide-mediated anal relaxation observed in the colon.<sup>17</sup> In contrast, the role of descending inhibitory pathways in the ileum remains unclear; reflex-evoked fast inhibitory junction potentials<sup>51</sup> might regulate propulsion by reducing the rate and strength of the anal contraction as it propagates down the bowel.<sup>20</sup>

During stimulation, new pacing sites are induced randomly (both spatially and temporally) in both muscle layers; consistent with the notion that although the sensory neurons and interneurons in the reflex pathways are likely to be common to both muscle layers, the excitatory motor neurons innervating each layer are different.<sup>1-3</sup> Neural stimulation causes frequent collisions between waves propagating in the short axis that originate from adjacent pacing sites, producing a more

synchronous excitation. This confinement of excitation to thin slivers of LM ensures that contractions occur at the same time around the gut to sum and produce uniform shortening of a segment of intestine.<sup>29</sup> In CM, collisions between induced neighboring bands of excitation promote stationary ring-like contractions that are confined to neurally excited regions along the short axis of the CM. Therefore, collisions between  $\text{Ca}^{2+}$  waves stop the spread of excitation through the muscle, ensuring that the nerves directly control the sequential activation of the CM along the intestine during peristalsis (Figure 9C). The rate of spread of the synchronous induction of pacing sites in both layers during a peristaltic wave, which travels at approximately 25–30 mm/s down the ileum,<sup>20</sup> is controlled by the speed of propagating neural activity within the reflex pathways of the enteric nervous system.

#### Conclusions

$\text{Ca}^{2+}$  waves occur independently in each muscle layer of the guinea pig ileum. A key factor for this independence is spike generation from multiple, discrete pacing sites (regardless of electrotonic spread or common slow wave generators between the muscles). This lack of coupling between muscles allows for independent movements during mixing. Neural induction of new pacing sites at the same time in each muscle allows for synchronized contraction of the 2 layers during peristalsis.

#### References

1. Smith TK, Bornstein JC, Furness JB. Convergence of reflex pathways excited by distension and mechanical stimulation of the mucosa onto the same myenteric neurons of the guinea pig small intestine. *J Neurosci* 1992;12:1502–1510.
2. Smith TK, Burke EP, Shuttleworth CW. Topographical and electrophysiological characteristics of highly excitable S neurones in the myenteric plexus of the guinea-pig ileum. *J Physiol (Lond)* 1999; 517.3:817–830.
3. Costa M, Brookes SJH, Steele PA, Gibbins I, Burcher E, Kandiah CJ. Neurochemical classification of myenteric neurons in the guinea-pig ileum. *Neuroscience* 1996;75:949–967.
4. Weems WA. Intestinal fluid flow: its production and control. In: Johnson LR, ed. *Physiology of the gastrointestinal tract*. 2nd ed. New York: Raven, 1987:571–593.
5. Wood JD. Mixing and moving in the gut. *Gut* 1999;45:333–334.
6. Bayliss W, Starling EH. Movements and innervation of the small intestine. *J Physiol (Lond)* 1899;24:99–143.
7. Weisbrodt NW. Motility of the small intestine. In: Johnson LR, ed. *Physiology of the gastrointestinal tract*. 2nd ed. New York: Raven, 1987:631–664.
8. Sarna SK. Gastrointestinal longitudinal muscle contractions. *Am J Physiol* 1993;265:G156–G164.
9. Melville J, Macagno E, Christensen J. Longitudinal contractions in the duodenum: their fluid mechanical function. *Am J Physiol* 1975;220:1887–1892.
10. Yokoyama S, North RA. Electrical activity of longitudinal and circular muscle during peristalsis. *Am J Physiol* 1983;244:G83–G88.
11. Kosterlitz HW, Lee GM. Pharmacological analysis of intrinsic intestinal reflexes. *Pharmacol Rev* 1964;16:301–339.
12. Kottegoda SR. An analysis of the possible nervous mechanisms

- involved in the peristaltic reflex. *J Physiol (Lond)* 1969;200:687-712.
13. Gregory JE, Bentley GA. The peristaltic reflex in the isolated guinea-pig ileum drug-induced spasm of the longitudinal muscle. *Aust J Exp Biol Med Sci* 1968;46:1-16.
  14. Wood JD, Perkins WE. Mechanical interactions between longitudinal and circular axes of small intestine. *J Neurophysiol* 1970;42:582-593.
  15. McKirdy HC. Functional relationship of longitudinal and circular muscle layers of the muscularis externa of the rabbit large intestine. *J Physiol (Lond)* 1972;227:839-853.
  16. Smith TK, Robertson WJ. Synchronous movements of the longitudinal and circular muscle during peristalsis in the isolated guinea-pig distal colon. *J Physiol (Lond)* 1998;506:563-577.
  17. Smith TK, McCarron SL. Nitric oxide modulates cholinergic reflex pathways to the longitudinal and circular muscle in the isolated guinea-pig distal colon. *J Physiol (Lond)* 1998;512:893-906.
  18. Garry RC, Gillespie JS. The response of the musculature of the colon of the rabbit to stimulation, in vitro, of the parasympathetic and of the sympathetic outflows. *J Physiol (Lond)* 1955;128:557-576.
  19. Spencer N, McCarron S, Smith TK. Sympathetic inhibition of ascending and descending interneurons during the peristaltic reflex in the isolated guinea-pig distal colon. *J Physiol (Lond)* 1999;519.2:539-550.
  20. Spencer N, Walsh M, Smith TK. Does the guinea-pig ileum obey the "law of the intestine"? *J Physiol (Lond)* 1999;517.3:889-898.
  21. Hennig GW, Costa M, Chen BN, Brookes SJ. Quantitative analysis of peristalsis in the guinea-pig small intestine using spatio-temporal maps. *J Physiol (Lond)* 1999;517:575-590.
  22. Yamamoto Y, Liu J, Smith TK, Mittal RK. Distension-related responses in circular and longitudinal muscle of the human esophagus: an ultrasonographic study. *Am J Physiol* 1998;275:G805-G811.
  23. Bortoff A. Electrical transmission of slow waves from longitudinal to circular intestinal muscle. *Am J Physiol* 1965;209:1254-1260.
  24. Connor JA, Kreulen D, Prosser CL, Weigel RI. Interaction between longitudinal and circular muscle in intestine of cat. *J Physiol (Lond)* 1977;273:665-689.
  25. Smith TK, Reed JB, Sanders KM. Interaction of two electrical pacemakers in muscularis of canine proximal colon. *Am J Physiol* 1987;252:C290-C299.
  26. Gabella G. Intercellular junctions between circular and longitudinal intestinal muscle layers. *Z Zellforschung Mikroskop Anat* 1972;125:191-199.
  27. Bywater RA, Taylor GS. Non-cholinergic excitatory and inhibitory junction potentials in the circular smooth muscle of the guinea-pig ileum. *J Physiol (Lond)* 1986;374:153-164.
  28. Horowitz B, Ward S, Sanders K. Cellular and molecular basis for electrical rhythmicity in gastrointestinal muscles. *Annu Rev Physiol* 1999;61:19-43.
  29. Stevens RJ, Publicover NG, Smith TK. Induction and organization of Ca<sup>2+</sup> waves by enteric nervous reflexes. *Nature* 1999;399:62-66.
  30. Stevens RJ, Weinert JS, Publicover NG. Visualization of origin and propagation of excitation in canine gastric smooth muscle. *Am J Physiol* 1999;277:C448-C460.
  31. Publicover NG, Smith TK, Stevens RJ. Fluorescent imaging of the propagation of excitability in gastrointestinal muscles. In: Bornhop DJ, Contag CH, Seveck-Muraca EM, eds. SPIE conference on molecular imaging: reporters, dyes, and instrumentation. San Jose, CA: Society of Photo-Optical Instrumentation Engineers, Washington, 1999:42-50.
  32. Ozaki H, Stevens RJ, Blondfield DP, Publicover NG, Sanders KM. Simultaneous measurement of membrane potential, cytosolic Ca<sup>2+</sup>, and tension in intact smooth muscles. *Am J Physiol* 1991;260:C917-C925.
  33. Smith TK, Furness JB. Reflex changes in circular muscle activity elicited by stroking the mucosa: an electrophysiological analysis in the isolated guinea-pig ileum. *J Auton Nerv Syst* 1988;25:205-218.
  34. Yuan SY, Furness JB, Bornstein JC, Smith TK. Mucosal distortion by compression elicits polarized reflexes and enhances responses of the circular muscle to distension in the small intestine. *J Auton Nerv Syst* 1991;35:219-226.
  35. Hirst GD, Holman ME, McKirdy HC. Two descending nerve pathways activated by distension of guinea-pig small intestine. *J Physiol (Lond)* 1975;244:113-127.
  36. Dickens EJ, Hirst GD, Tomita T. Identification of rhythmically active cells in guinea-pig stomach. *J Physiol (Lond)* 1999;514:515-531.
  37. Hirst GDS. A calcium window on the gut. *Nature* 1999;399:16-17.
  38. Cousins HM, Edwards FR, Hirst GD, Wendt IR. Cholinergic neuromuscular transmission in the longitudinal muscle of the guinea-pig ileum. *J Physiol (Lond)* 1993;471:61-86.
  39. Yokoyama S, Osaki T. Contractions of the longitudinal and circular muscle of the small intestine. *Prog Clin Biol Res* 1990;327:482-492.
  40. Bulbring E, Burnstock G, Holman ME. Excitation and conduction in the smooth muscle of the isolated taenia-coli of the guinea-pig. *J Physiol (Lond)* 1958;142:420-437.
  41. Smith TK. Spontaneous junction potentials and slow waves in the circular muscle of isolated segments of guinea-pig ileum. *J Auton Nerv Syst* 1989;27:147-154.
  42. Hara Y, Szurszewski JH. Effect of potassium and acetylcholine on canine intestinal smooth muscle. *J Physiol (Lond)* 1986;372:521-537.
  43. Bolton TB. On the nature of the oscillations of the membrane potential (slow waves) produced by acetylcholine or carbachol in intestinal smooth muscle. *J Physiol (Lond)* 1971;216:403-418.
  44. Spect PC. Propagation of stimulated slow waves in cat intestinal muscle. *Am J Physiol* 1976;231:228-234.
  45. Schanne FA, Kane AB, Young EE, Farber JL. Calcium dependence of toxic cell death: a final common pathway. *Science* 1979;206:700-702.
  46. Choi DW. Still center-stage in hypoxic-ischemic neuronal death. *Trends Neurosci* 1995;18:58-60.
  47. Nagai T, Prosser C. Patterns of conduction in smooth muscle. *Am J Physiol* 1963;204:910-914.
  48. Barr L, Dewey M, Berger W. Action potentials can propagate along small strands of smooth muscle. *Pflugers Arch* 1979;380:165-170.
  49. Hara Y, Kubota M, Szurszewski JH. Electrophysiology of smooth muscle of the small intestine of some mammals. *J Physiol (Lond)* 1986;372:501-520.
  50. Frigo GM, Torsoli A, Lecchini S, Falaschi CF, Crema A. Recent advances in the pharmacology of peristalsis. *Arch Int Pharmacodyn Ther* 1972;196(suppl):9-24.
  51. Hirst GD, McKirdy HC. A nervous mechanism for descending inhibition in guinea-pig small intestine. *J Physiol (Lond)* 1974;238:129-143.

---

Received August 9, 1999. Accepted January 13, 2000.

Address requests for reprints to: Terence K. Smith, Ph.D., Department of Physiology and Cell Biology, MS 352, University of Nevada School of Medicine, Reno, Nevada 89557. e-mail: tks@physio.unr.edu; fax: (775) 784-6903.

Supported by a grant from the National Institutes of Health, NIDDK 45713 (to T.K.S.).